# Integrated interpretation of most positive and most negative curvature of ground gravity data across the Shillong plateau and Mikir hills periphery, north-east India

**Gopal K. Ghosh** ( gk_ghosh@yahoo.com )
Oil India Limited

**Research Article**

**Keywords:** Shillong plateau, Gravity, Most positive curvature, Most negative curvature, Thrust-fault, Lineament

**Posted Date:** July 28th, 2022

**DOI:** https://doi.org/10.21203/rs.3.rs-1882957/v1

# Integrated interpretation of most positive and most negative curvature of ground gravity data across the Shillong plateau and Mikir hills periphery, north-east India

**Gopal K. Ghosh**[1]

[1]Email: gk_ghosh@yahoo.com

Geophysics Department, Oil India Limited, Duliajan, Assam, India

## Abstract

The study area falls in one of the utmost seismically vigorous zones covering latitude 23°–28°N and longitude 88°–96°E in the north-eastern part of India. Various studies suggest that tectonic activities are still active across the Shillong plateau, Mikir hills, Arakan-Yoma fold belt, Naga hills, parts of Bengal basin, lower-upper Brahmaputra valley along with the Mishmi hills of Himalayan foothills. The available information about the thrust-faults in the area is very limited and most of the information are available from the geographic information system map, field geological studies and very limited from seismic and other data sources. In this present study, attempt has been made to carry out details study of most positive and most negative curvature attributes for understanding sub-surface structural features and able to identify structural lineament/thrust-fault in the study area using available ground gravity data in the north-eastern part of India. Further, present studied results are correlated and compared with the past derived results of three-dimensional Euler source depth locations and source edge estimations in this area. The integrated results of the curvature interpretation look promising and can able to delineate the thrust–fault locations. This paper also suggests

additional new thrust-fault lineament information. As the gravity data has its own constraint hence integrated study can help to provide for better geoscientific information.

**Keywords.** Shillong plateau; Gravity; Most positive curvature; Most negative curvature; Thrust-fault; Lineament.

## Introduction

The area of study falls under Shillong-plateau and Mikir hills complex situated in one of the most seismically dynamic zones ranging latitude 23°–28°N and longitude 88°–96°E. Studies suggest that subsurface tectonic are still active across the Shillong plateau, Mikir hills, Arakan-Yoma fold belt, Naga hills, parts of Bengal basin, lower-upper Brahmaputra valley along with the Mishmi hills of Himalayan foothills (**Hazarika et al., 2022; Shukla et al, 2022**). The available information about the thrust-faults is very limited and most of the information are available from the geographic information system (GIS) map, others field geological studies and very limited from seismic and other geoscientific data sources. Various studies suggest that the area is still active as per the latest occurrences of earthquake locations in the north-eastern India and its adjoining areas is shown in **Figure 1.**

Gravity maps are frequently analysed for delineating the geological contact and subsurface information. These gravity maps have signals originating from the different geometries situated at particular depth with different density properties. Present study deals with advance curvature attribute interpretation for studying geological information using available ground gravity data **(Verma and Mukhyopadhyay, 1977)** across the Shillong-plateau Mikir-hills periphery, north-eastern part of India. Most positive and most

negative curvature interpretation deliver a good outcome and able to delineate the thrust–fault locations. The derived results from this study are correlated with the previously finding results of three-dimensional Euler deconvolution for source depth locations (**Ghosh, 2022)** and source edge estimation (SED) technique by **Ghosh (2019).**

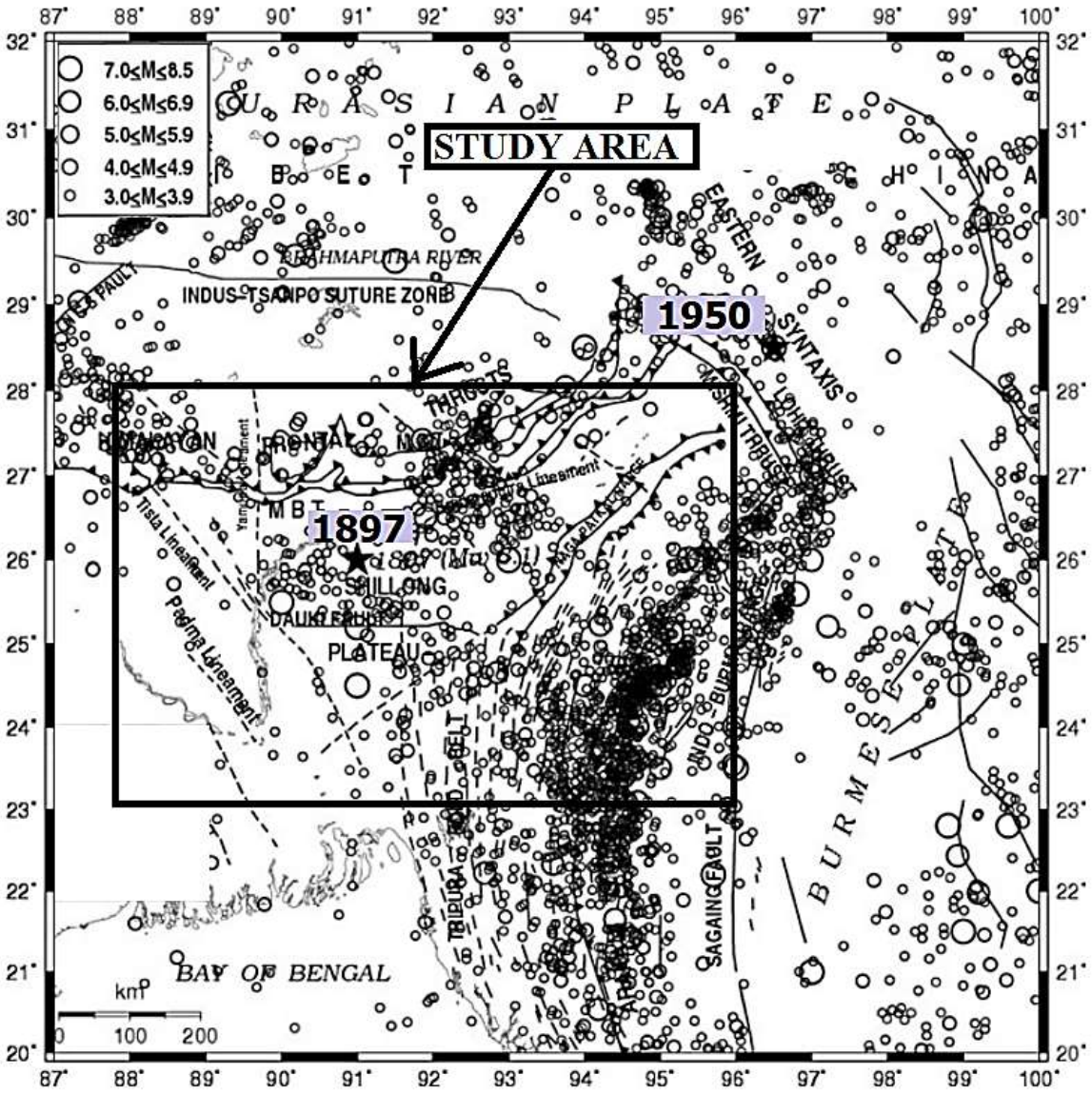


Fig. 1. Map shows the latest earthquake distributions across the north-eastern India and adjoining region (**after Yadav et al., 2009**). Study area is marked by the rectangular box. Two major earthquake locations held on 1950 and 1897 have marked with "∗".

The study suggests that, most positive and most negative curvature have played a significant role to understand sub-surface structural features and able to identify structural lineament in the north-eastern part of India. As the gravity data has been acquired in 1977 has its own limitation, despite of these, the curvature output results are providing a significant role and highlighting major thrust-fault locations. Studies also suggests that there are some additional thrust-fault locations which are not previously identified are also marked here. The patterns of colour contrast plots of different curvatures are providing to understanding the detail's information in this area.

## Geological and Tectonic setting

The study area is covered with north-eastern Himalaya towards north, Bengal Basin towards south and Indo-Burma ranges towards east. It is understood that Himalayan collision belt was due to the ongoing thrusting of Indian plate towards the Eurasia plate. In northeast India, three major plates interact along two convergent boundaries: the Himalayas and the Indo–Burma Ranges, which meet at the Assam Syntaxis. The collision between the Burmese and Indian plate act towards south-east direction and studies suggest that south-eastern parts further extended towards Andaman-Sumatra region. Such kind of plate movement originate a complex intra-plate distortion and produces high seismic activity zone **(Bansal and Verma, 2013**).

**Harijan et al., (2003)** suggested that the Shillong plateau is still active with counter clockwise movement of Indian plate against the Eurasian plate. It may be incurred that tectonic resettlement causing upliftment of the Shillong plateau may cause for gravity

variation and changes in altitude varying up to 2000m and an average elevation is 1000m above mean sea level. These changes happen mostly in between Brahmaputra Thrust (BT) and the Dauki Fault (DF). It is implied that the tectonic resettlement causes generation of various thrusts-faults activities in this study area. The most prominent thrust/faults are Tista faults (TF), Dapsi thrust (DpT), Kopili faults (KF), Jorhat fault (JF), Kabaw fault (KbF), Sylhet fault (SF), Oldham faults (OF), Dhubri fault (DhF), Naga thrust (NT) and Disang thrust (DiT) present this area (**Fig. 2**). Many researchers **(Rao et al., 2006)** also suggested that occurrences of 1950 and 1897 earthquakes are also playing major role to impact north-eastern India (**Fig. 1**).

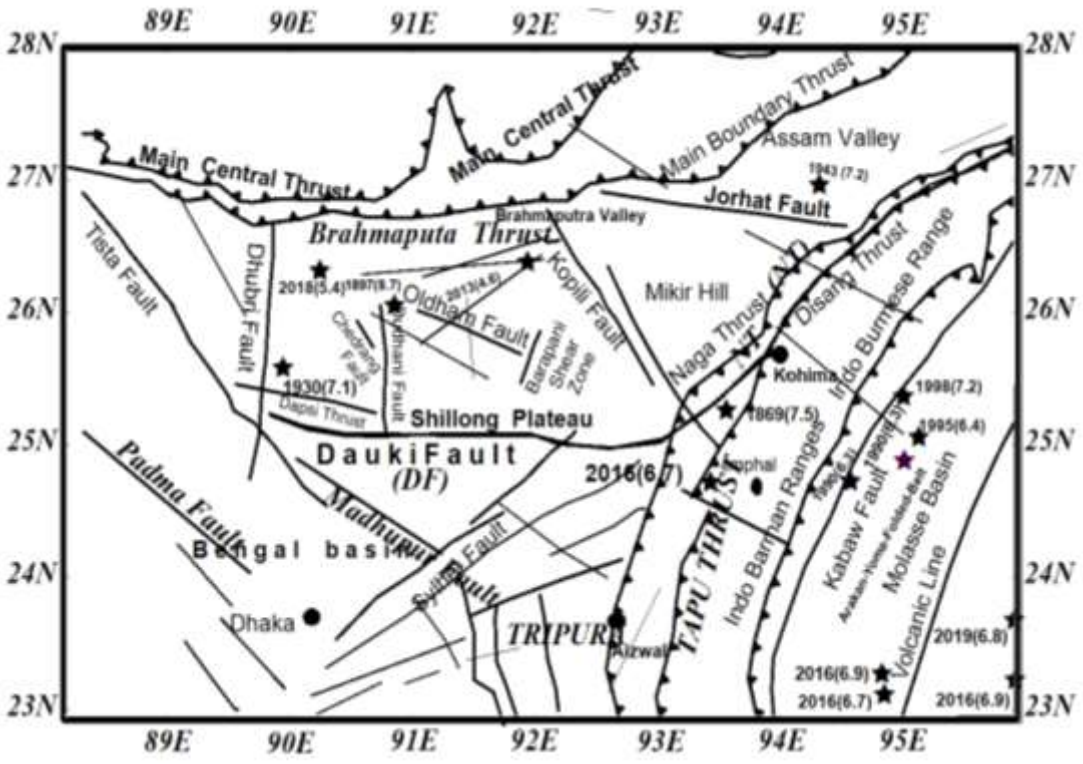


Fig. 2 Map shows the various thrust-fault locations in the study area. The major earthquake's locations are marked in "∗" with its magnitude. A Simplified geological map of the north-eastern India and its surroundings are indicating various locations of boundaries, thrusts, faults, rivers, suture zone, etc. has shown in **Figure 3 (Robinson et al., 2014 and Awasthi et al., 2014, Ghosh, 2019).**

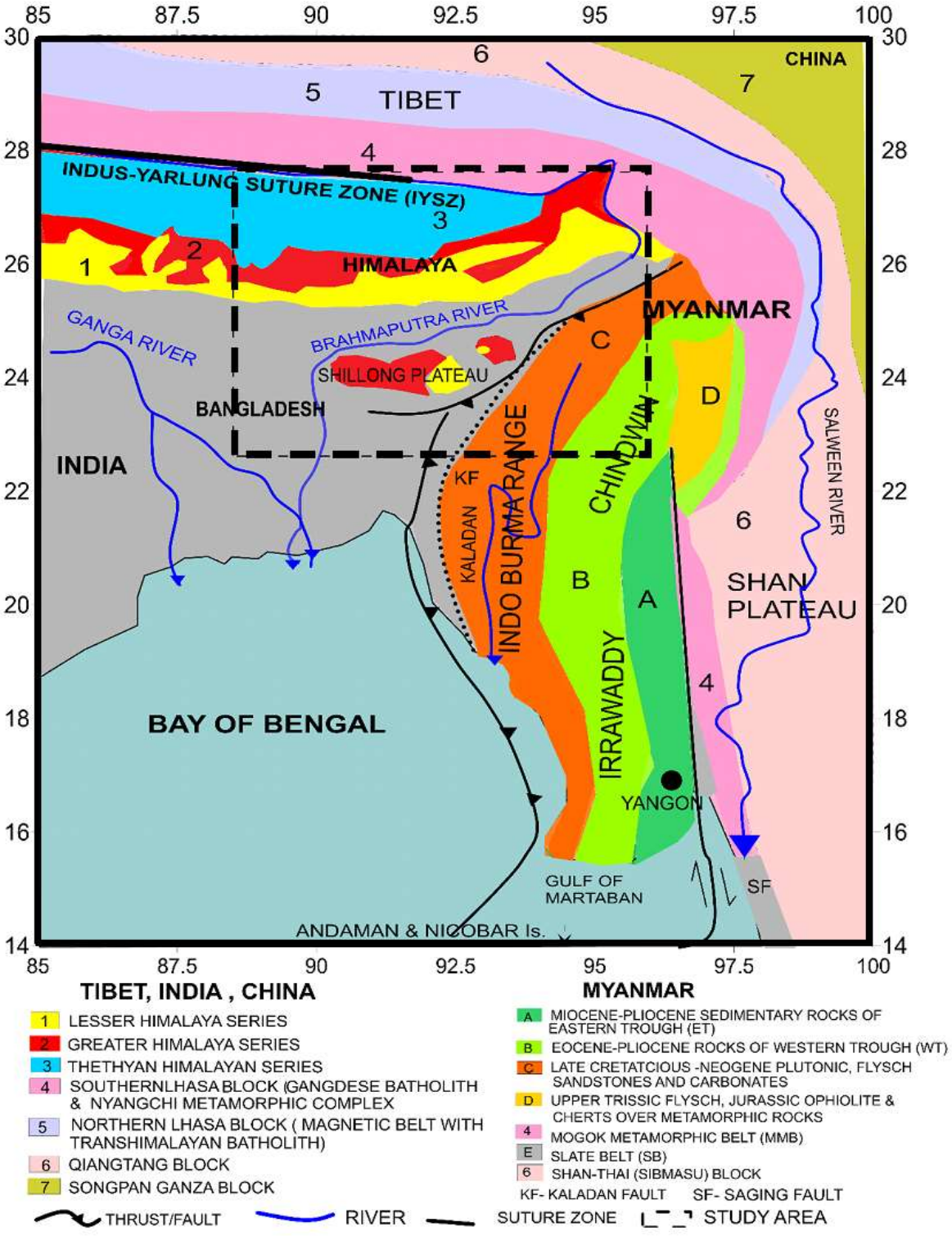


**Fig 3**. Simplified geological map of the northeast India and its surroundings indicating various locations of boundaries, thrusts, faults, rivers, suture zone, etc. (after **Robinson et al. 2014; Awasthi et al. 2014, Ghosh, 2019**).

105 The north-dipping of the DF and the south-dipping of OF are the key features for pop-
106 up tectonic structure associated with the earthquake's activities (**Bilham and England**
107 **(2001)**. This pop-up structures reasons for the doubly arranging fold system (**McClay**
108 **and Bonora, 2001; Schellart and Nieuwland, 2003**). The collision of the Eurasian
109 plate and the Indian plate triggered by subduction beneath the Burmese plate at the
110 Himalayan zone (**Seno and Rehman, 2011).** There is an indicative convergence arc in
111 between the Burmese arc and the Shillong-plateau are concerned in the dissimilar
112 direction caused by the tectonic disorders instigated by the Himalayan collision zone
113 and Indo-Burma subduction zone (**Rajesekhar and Mishra, 2008 and Kayal, 2001).** It
114 was suggested that Mikir-hills was a fragmented part of the Shillong plateau caused the
115 by the Kopili fault and the and large earthquake (**Oldham, 1889; Nandy** and **Dasgupta,**
116 **1991; Ambraseys** and **Douglas, 2004).**

117 Various types of geological formations encompass meta sedimentary Shillong group
118 **Rock (1530-1550) m**, porphyritic granites and ultramafic alkaline-carbonate complexes,
119 Archean Gneissic Complex (Archaean Rock) and igneous rocks **(Evans, 1964; Mitra,**
120 **1998; Mishra and Sen, 2010; Devi and Sarma, 2010).** Studies suggest that the
121 thickness of Sylhet area southwards of the DF is varying 13-18 km from the Tertiary to
122 the recent time **(Biswas and Grasemann, 2005; Evans, 1964; Ghosh, 2015).**
123
124 Further, it is suggested that Cretaceous-Tertiary sediments are located in the southern
125 part of the Shillong plateau. Assam valley also comprises majority of the sedimentary
126 rocks at varied ages like upper Precambrian-lower Proterozoic, Tertiaries and
127 Gondwana rocks. It is also stated that OF is 110 km long and oriented towards NW-SE
128 direction. The OF is dipping at an angle about $57^0$ and submerges 9 km to 45 km

beneath the Shillong plateau. However, **Bilham and England (2001)** articulated that the OF might be "Cryptic" reverse fault prolonged towards the northern boundary of the Shillong plateau. It is also expected that the **BT** is situated in the northern part of the OF (**Rajendran et al., 2004 and Kayal et al., 2006).**

## Qualitative interpretation of Bouguer gravity data

The gravity survey was acquired by the various Institutes including Oil and Natural Gas Corporation (ONGC), National Geophysical Research Institute (NGRI), Oil India Limited (OIL), Assam Oil, Geological Survey of India (GSI) etc. in the year 1977 using Worden gravimeter maintaining a grid interval of 1000m to 3000m in this area and the same has been published by **Verma and Mukhopadhyay (1977).** Further**, Ghosh et al., (2015)** and **Ghosh (2019)** digitized the Bouguer gravity data with a fair degree precision **(Fig. 4**) for further interpretation.

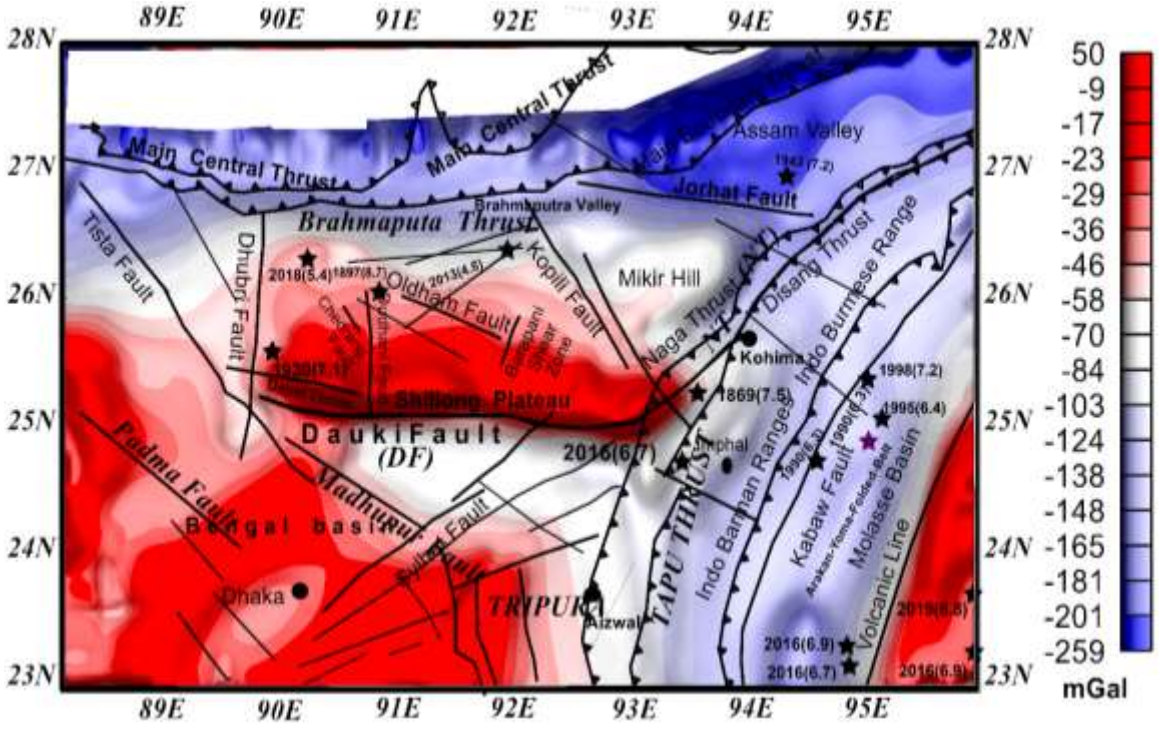


**Fig. 4.** Map shows the Bouguer gravity anomaly ranging from -259 mGal to +50 mGal in the study area (after **Verma and Mukhopadhyay,1977**; **Ghosh et al., 2015**).

Further interpretation for delineating the thrust-fault location has been carried out using curvature interpretation. Shillong plateau is enclosed by a steep gravity gradient contour trending in a structural trend. It is studied that the major contours are oriented north-east south-west orientation in the eastern part, east-west trending in the northern part, north-south trending in the southern part and south-west north-east trending in the south-western part of the area. Gravity anomaly suggests that the These steep contours are situated at south-west north-east of NT, east-west of BT, east-west of DF, east-west of JF, north-south of DhF and north-west south-east of KF. Assam and Brahmaputra valley, Molasse basin and parts of the south-eastern part of Bengal basin are fall under low gravity whereas, south-western part of the Bengal basin and the Shillong plateau fall under higher gravity zone. It is observed that, the Shillong plateau has higher gravity with higher elevation and the Bengal basin observed higher gravity with lower elevation (**Fig 4 and 5**).

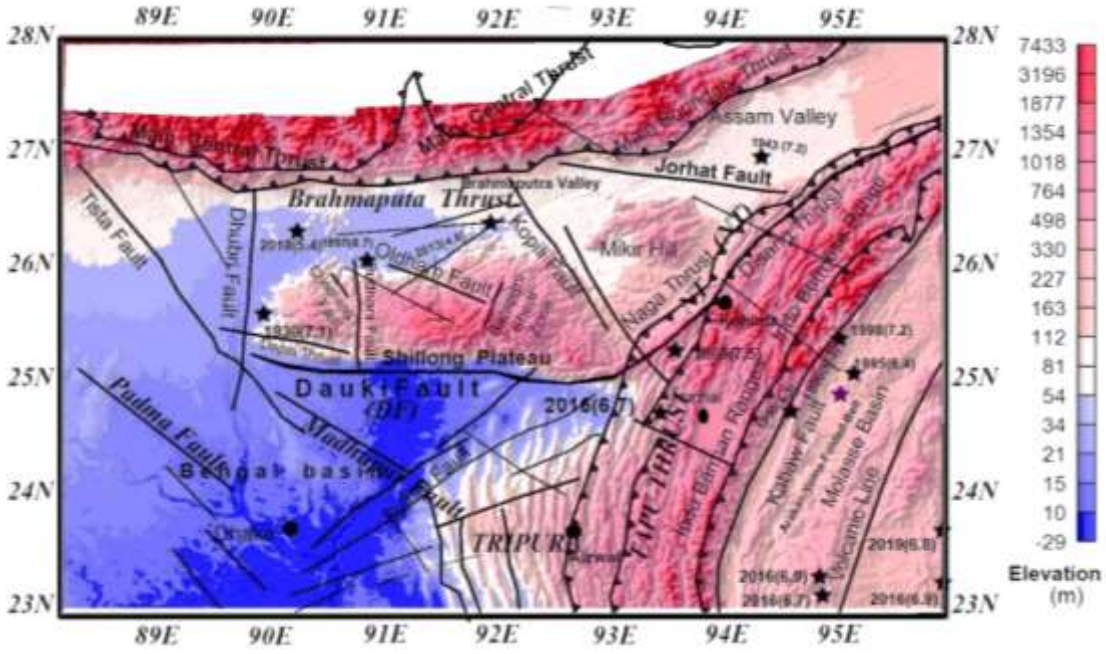


**Fig. 5**: Map shows the surface elevation of the study area, Molasses basin and main boundary thrust areas.

The lower elevation observed at Bengal basin, Assam shelf and northern part of Shillong plateau. However, higher gravity anomaly located at the Shillong plateau and Bengal basin consisting comparatively deeper formations with higher density rock. This type of gravity and elevation variation might be explained as mass deficiency. Further, it is observed that lower gravity areas (main central thrust and Molasse basin) covering thicker sedimentary rock with lesser density formation. This can be explained as isostatic adjustment. Present study deals with the curvature interpretation for thrust-fault locations and structural delineation. As the study area falls under highly active tectonic zone this might cause continental upliftment / depression in this area.

**Mathematical approach of curvature**

Curvature can be mathematically defined as the inverse of the radius (1/r). The larger curvature produces larger rate of change. **Thomas (1972)** states about the curvatures measure how fast the curve is changing direction at a point such as surface deviation from being a flat plane or any part of continuous curve**.** Curvature interpenetration has established useful delineation of fault-fracture and orientation pattern using geoscientific data. Present study deals with the different types of curvature results for identifying thrust-faults information. Curvature analysis has been utilised earth's gravitational field as a geoid surface (represented as an equipotential earth surface) from mean sea level. The Schematic diagram of different curvatures in a 2D space has shown in **Figure 6.** The arrows are the normal to the continuous curv surface (**Figure 6**). The Converging arrows (syncline) show negative curvature, parallel vectors show flat arrows representing zero curvature and diverging arrows (anticline) show positive curvature. Flat planes are indicated as a parallel vector representing zero curvature. Positive

curvature (anticline) indicates with diverging nature and negative curvature (syncline) represented as converging nature (**after Robert, 2001).**

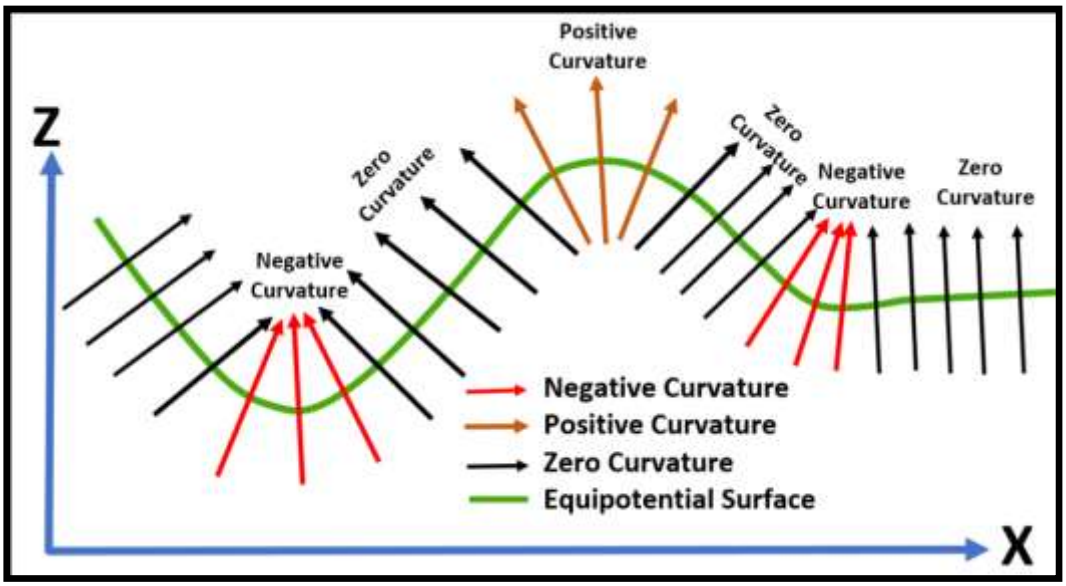


**Figure. 6**. Schematic diagram of a two-dimensional space showing normal to the curved surface. The converging arrows (syncline marked in red arrows) show negative curvatures, parallel vectors (flat arrows marked in black arrows) are zero curvature and diverging arrows (anticline marked in violet arrows) shows positive curvatures.

Bouguer gravity data has been used as a continuous potential field dividing into three components namely eastern component (Gx), northern component (Gy) and vertical component (Gz). A detailed cartesian coordinate system for an equipotential surface has been explained by **Slotnick (1932).** Positive and negative curvatures are located in an anticline and syncline surface and zero curvature is shown in the no dip plane or in the flat surface as shown in **Figure 6** represented in the two-dimensional surface.

To derive the curvature equation a new function $P(x, y, z)$ is considered which represents a continuous equipotential function expressed as a gravitational potential. Second order gravity derivatives with respect to x and y components (Pxx, Pyy, Pxy or Pyx) have been produced from the first order gravity derivative components (Px, Py). These second order gravity derivatives are named as curvature gradients. Second order gravity gradients are basically represented as a quadratic approximation surface. Accordingly, the solution against the nonlinear second-degree gridded surface can be determined by using least square equation as written in equation (1),

$$P(x, y, z) = \alpha x^2 + \beta y^2 + \gamma xy + \delta x + \eta y + \sigma \quad (1)$$

where,

*P*(*x,y,z*) is the continuous equipotential function termed as gravitational potential;

α, β, γ, δ, η and σ are the various coefficients and can be written as shown in equation (2), where,

$$\alpha = \frac{\partial^2 P(x, y, z)}{2\partial x^2};\ \beta = \frac{\partial^2 P(x, y, z)}{2\partial y^2};\ \gamma = \frac{\partial^2 P(x, y, z)}{\partial x \partial y};\ \delta = \frac{\partial P(x, y, z)}{\partial x};\ \eta = \frac{\partial P(x, y, z)}{\partial y} \quad (2)$$

Mathematically, rearranging the coefficients of α, β, $\gamma$ and $\delta$ from equation (2) and substituting coefficient η equal to zero in equation (1), most positive curvature ( $K_+$ ) (**Young, 1978)** can be expressed using as shown in equation (3)

$$K_+ = (\alpha + \beta) + \sqrt{(\alpha - \beta)^2 + \delta^2} \quad (3)$$

Similarly, the most negative curvature ( $K_-$ ) (**Young, 1978)** is expressed as in equation (4) using coefficient η equal to zero in equation (1) and rearranging the coefficients of α, β, $\gamma$ and $\delta$ from equation (2) as shown in equation (4)

$$K_- = (\alpha + \beta) - \sqrt{(\alpha - \beta)^2 + \gamma^2} \qquad (4)$$

The $K_+$ and $K_-$ exaggerate domes and basinal features on the surface.

In a continuous plot there might be several local minimas or maximas, however, there will be one global minima and one global minima as shown in **Figure 7**. Curvature analysis are to be implied for cosidering global maxima and global minima points in a potential curve. Therefore, in the case of most positive curvature and most negative curvature in a potential curve only a single point in the curve will be locted for maxima or minima.

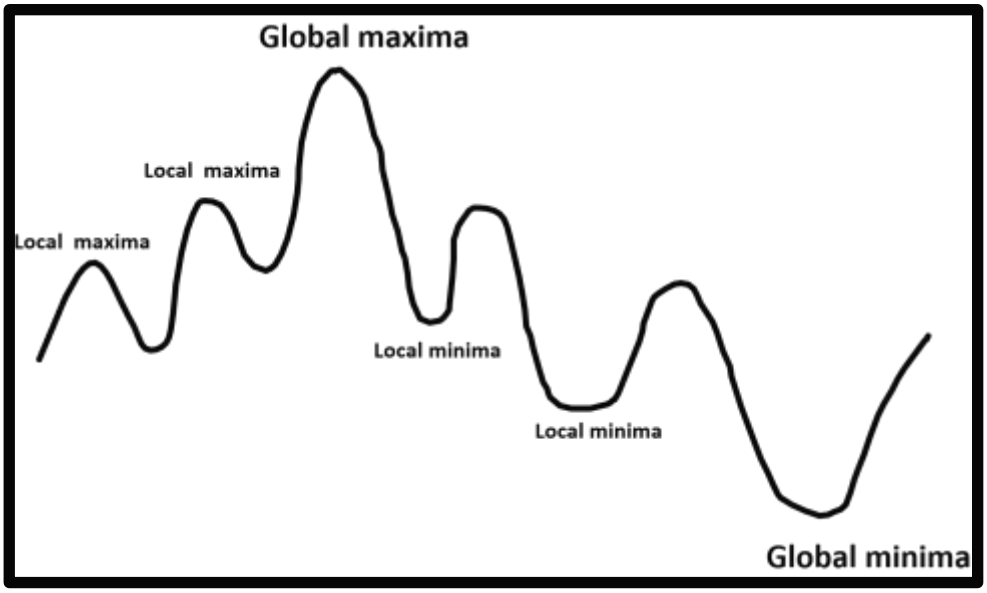


Fig 7. Map shows the representation of local minima, local maxima, global minima and global maxima.

Application for detailed curvatures analysis for understanding geological consequences have been discussed in details using potential field data by **Peet and Sahota (1985); Lee et. al., (2012); Li (2015); Ghosh (2018, 2020); Ghosh et al., (2017).**

## Gravity data interpretation

Thrusts and faults have a very significant role for understanding the structural and stratigraphic setup. As the study area is very much prospective in oil and gas resources and hence the development, evolution and formation of thrust and faults and their control on the migration and accumulation of hydrocarbon are very much important. It is well known that seismic methods can provide better information of geological structures. Most part of the study area are not accessible due to the geologically complex, hilly, thrust-fold belt, mountain, riverbed and dense forest covered areas. Although, some portions are accessible and conducted survey but lacking details information as a whole. In recent past, gravity survey was carried out by the various Institutes and data was published by **Verma and Mukhopadhyay (1977)**. Attempt has been made to use the Bouguer gravity data by various workers and mostly studied with two-dimensional approach in the recent past **(Khan and Chakraborty, 2007; Roy, 2008; Rajshekhar and Mishra, 2008; Ghosh et al., 2015, Ravi Kumar et al., 2020;**). However, recently researchers are using latest techniques like three-dimensional Euler source depth locations (**Yaghoobian et al., 1992; Silva and Barbosa, 2003; Mikhailov et al., 2003; FitzGerald et al., 2004; Ghosh, 2016b; Reid et al., 2003; Reid et al., 2014 ; Ghosh 2022)**, source edge estimations (SED) (**Wang et al., 2009; Ghosh, 2019; Ghosh 2016a; Ghosh et al., 2013; Thurston and Smith, 1997**), 2½-dimensional modelling using Marquardt's inversion (**Ghosh and Singh, 2011; Ghosh et al, 2010),**

**curvature analysis (Slotnick 1932; Robert, 2001; Ghosh, 2018; Fedi, 2007; Ghosh 2020;**), TILT and TDX derivative (**Fairhead et al., 2011; Salem et al., 2007; Ghosh, 2019)**, Cos(θ) analysis (**Wijns, 2005; Ghosh, 2019; Ghosh et al., 2015**) and various gravity gradient analyses (**Klingele et al 1991; Ghosh et al., 2017; Marson et al 1993 ; Saibi et al., 2006**) for getting advance subsurface information.

In this study area, attempt has been made to work for most positive and most negative curvature analysis using Bouguer gravity data (Verma and Mukhopadhyay, 1977) and thereafter correlating with the previous workout results**. Figure 8** indicated the source depth locations plots derived from three-dimensional Euler deconvolution of gravity data in this study area superimposing on the tectonic map of the area (**Ghosh, 2022).** The various source depth locations are marked with different coloured circle where depths are varying from < 4 km, 4-6 km, 6-8 km, 6-8 km and more > 8 km. Various marked circles are indicating the source depth locations and cluster data points are indicating the probable orientation of thrust-fault **Ghosh (2022**). Further, the most positive and most negative curvature result will be correlated in the next section.

Correspondingly, both the Euler deconvolution map for source depth locations (**Fig.8) (Ghosh 2022)** and the source edge locations map (**Fig. 9**) (**Ghosh, 2019**) are superimposed as shown in **Figure 10** on the tectonic map of the area containing various thrust-fault and major earthquake locations.

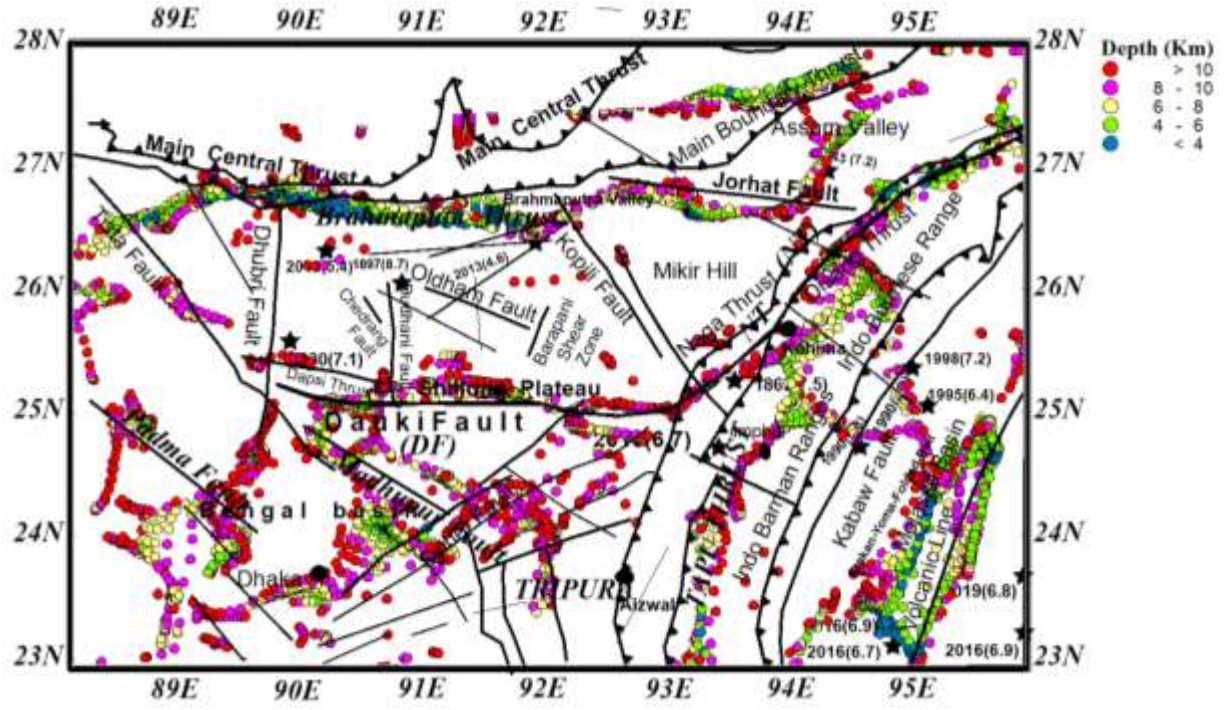


Fig. 8. Map shows the source depth locations derived from three-dimensional Euler deconvolution of gravity data. Various colour circles are indicating the source depth locations and the cluster data points are indicating the probable orientation of thrust-fault (**after Ghosh 2022**).

**Figure 9** indicates the source depth locations plot superimposed on the tectonic map of the area. The various strikes and dips are indicated tin the red colour **(Ghosh 2019).** Most positive curvature ($K_+$) has been calculated using equation (3), the coefficients indicated in equation (2) are substituted in equatuin (3). **Figure 11** shows the most positive curvature plot indicating the greatest positive values (marked in purple colour) indicating the anticlinal and dome shaped feature. The purple colour contract shows a good correlation of thrust-fault locations with the previously marked tectonic plot (**Fig 2.)**

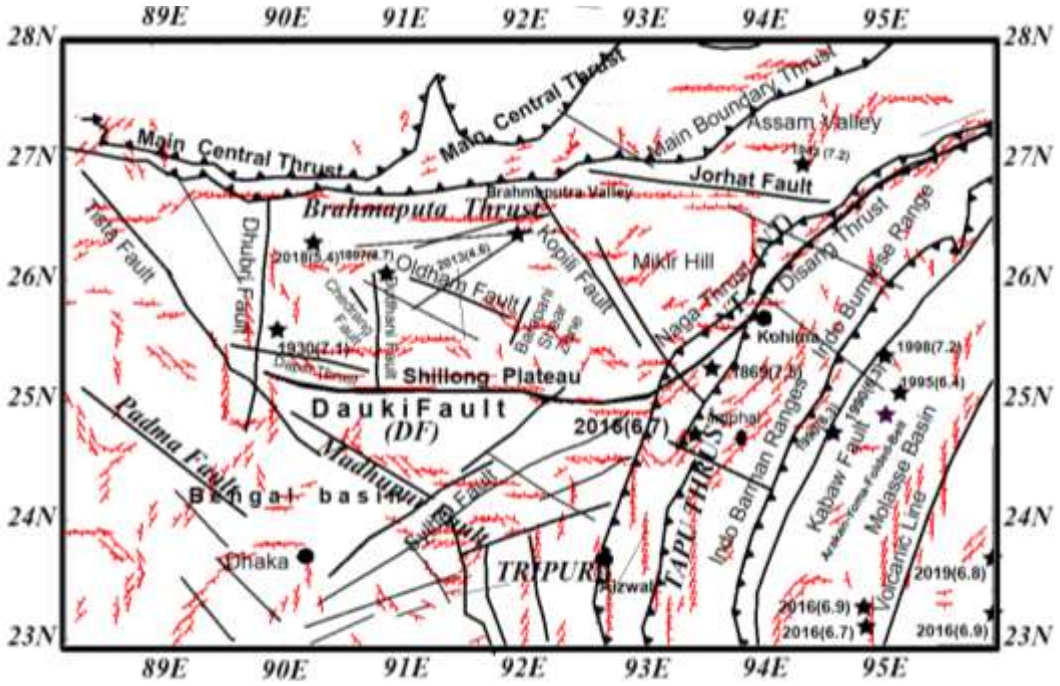


Fig. 9. Map shows the source edge locations indicating the strike and dip direction. The orientation cluster pattern indicating the probable orientation of thrust-fault (after **Ghosh 2019**).

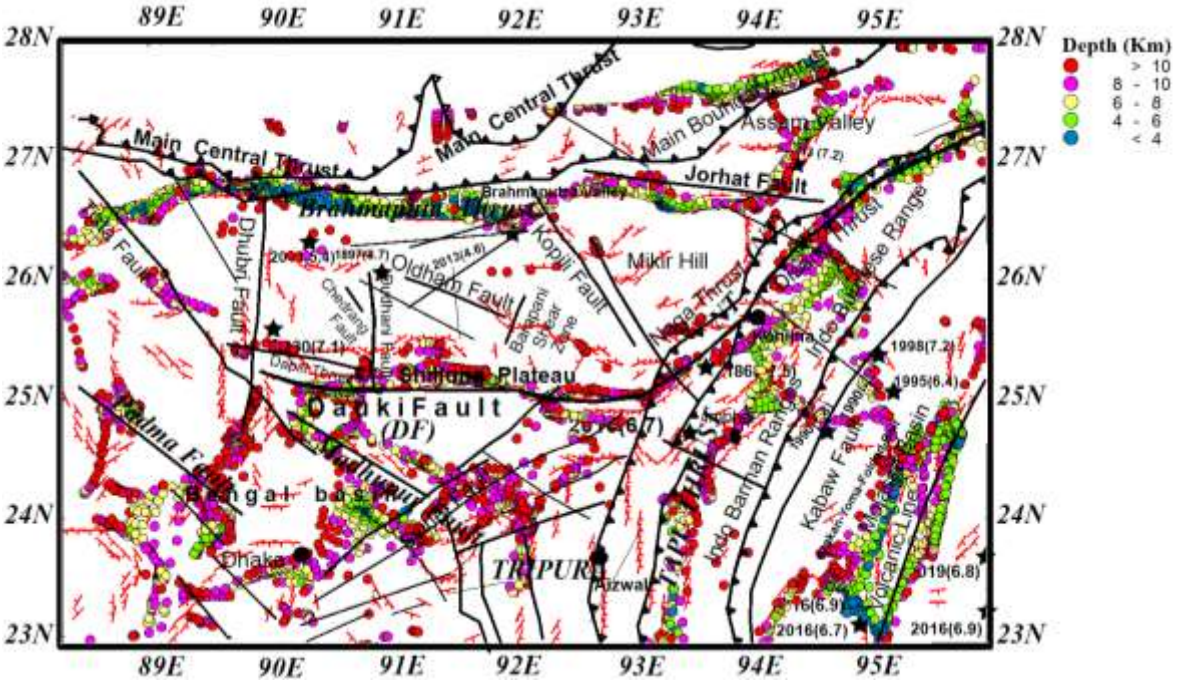


Fig. 10. Map shows the superposition of both the three-dimensional Euler source depth locations and the source edge locations plots on the tectonic map containing various thrust-fault including major earthquake locations.

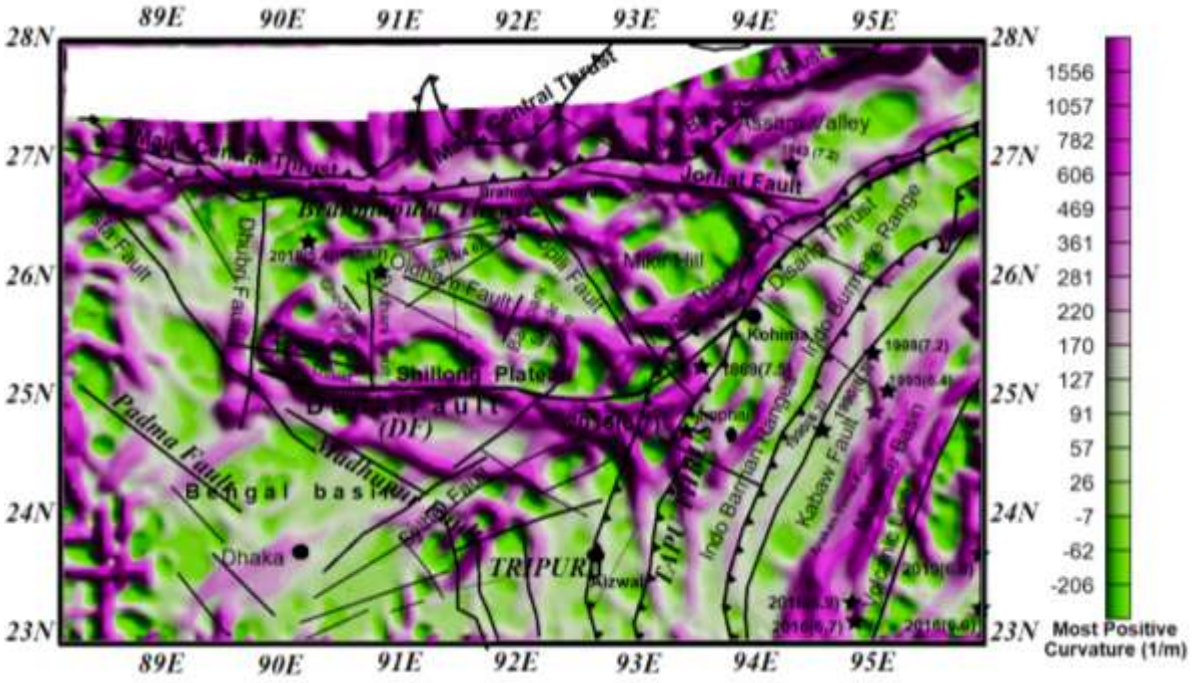


Fig. 11. Map shows the most positive curvature plot indicating the greatest positive values (marked in purple colour) indicating the anticlinal and dome shaped feature. The most positive curvature plot is superimposed on the tectonic map. Study suggests that the purple colour contract patterns are matching along with the thrust-fault locations.

Further, the derived results of the most positive curvature in the present study is compared and superimposed with the past derived Euler source depth location results (marking wjite lines) as shown **Figure 12.** Study suggests that the purple color contract patterns are matching along with the thrust-fault loactions as stated in the tectonic map (**Fig. 2**). Likewise, the most positive curvature results are superimposed to the past derived results of source edge location as shown in **Figure 13 ( Ghosh 2019).** The source edge location parrerns along with the strike directions are well correlating with most positive curvature plot. Further, the integrated plot of most positive curvature (**Fig. 11**), source edge locations (**Fig. 12**), Euler source depth locations (**Fig 13**) are plotted

in an integrated map as shown in **Figure 14** for comparision and correlation purpose. It is observed that the most positive curvature results are very much helpful and well correlationg for direct source depth/thrust-fault dileation.

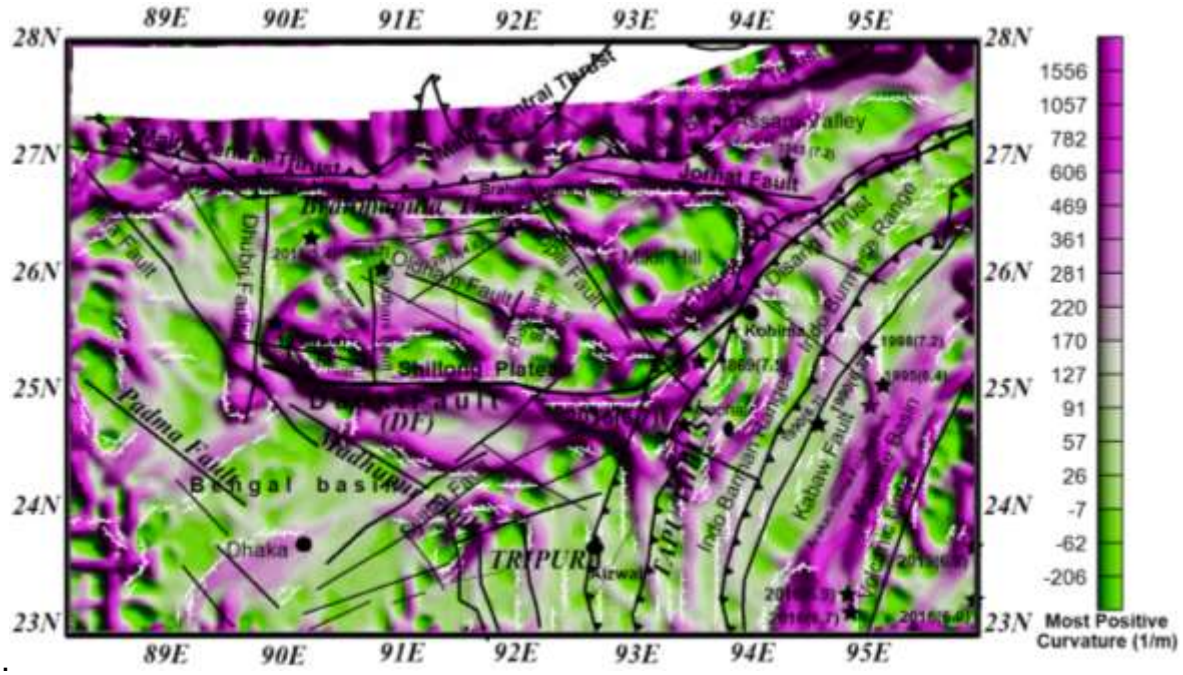


Fig. 12. Map shows source edge locations (marked with white lines) (**Ghosh, 2019)** superimposed on the most positive curvature plot.

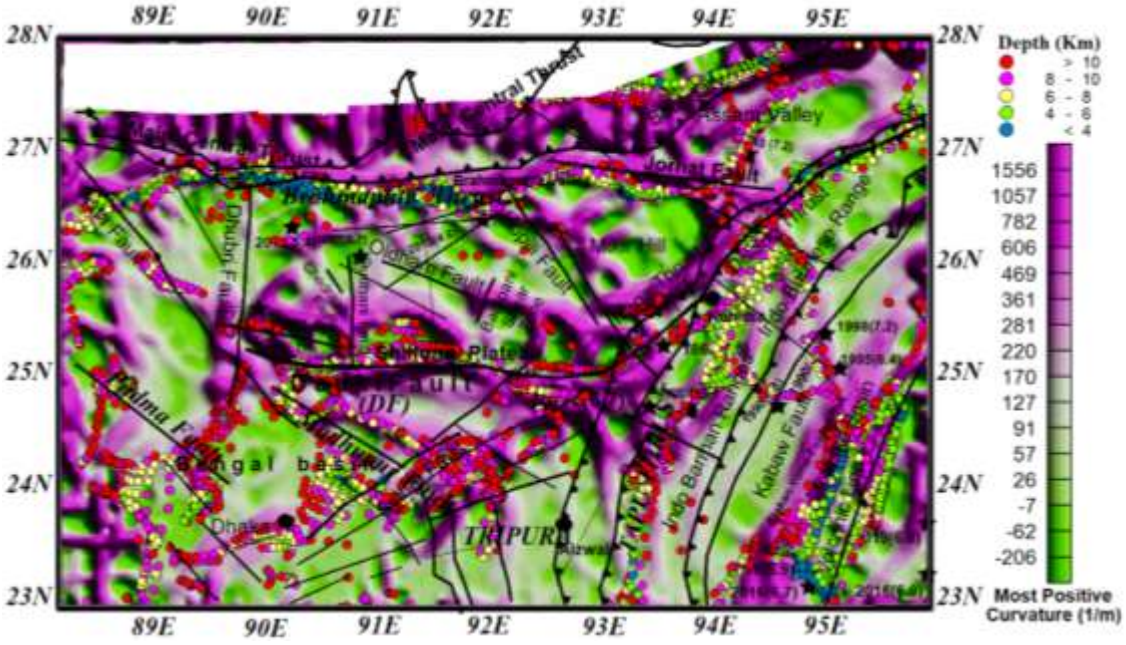


Fig. 13. Map shows the three-dimensional Euler source depth locations (**Ghosh, 2022)** superimposed on the most positive curvature plot and the results show well correlating.

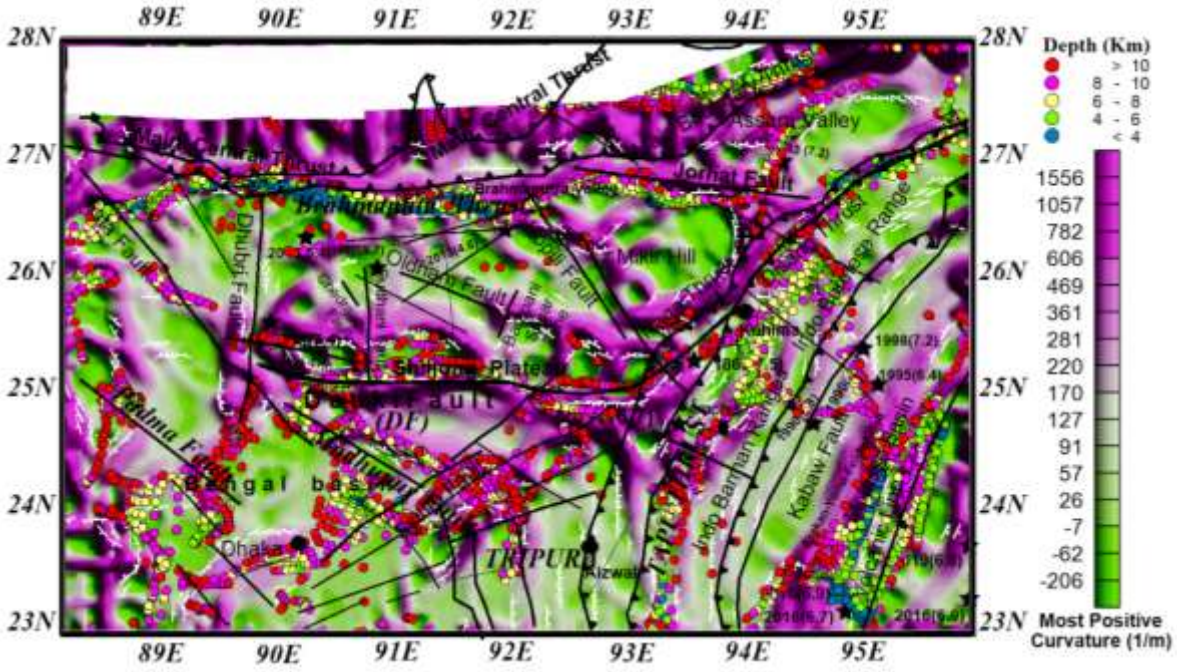


Fig. 14. Map shows the most positive curvature plot superimposed on the source edge location plot (marked in while lines) and three-dimensional Euler source depth locations ( marked in various colour circles).

In the similar way, most negative curvature( $K_{-}$ ) (marked with the green colour) has been plotted and superimposed on the tectonic map **(Fig. 15**). The synclinal and basin shaped feature show the most negative curvature as the gfreatest negative value (marked as green colour). The color contract pattern demonstrates a good connotation of thrust-fault locations over the most negative curvature plot. Further, for correlation and comparative analysis, most negative curvature are compared to the the past derivd results of source edge locations as shown in **Figure 16 (Ghosh , 2019).** Again the reuslts of most negative curvature plot has been compared with the past derived results of three-dimensional Euler source depth location as shown in **Figure 17(Ghosh, 2022)**.

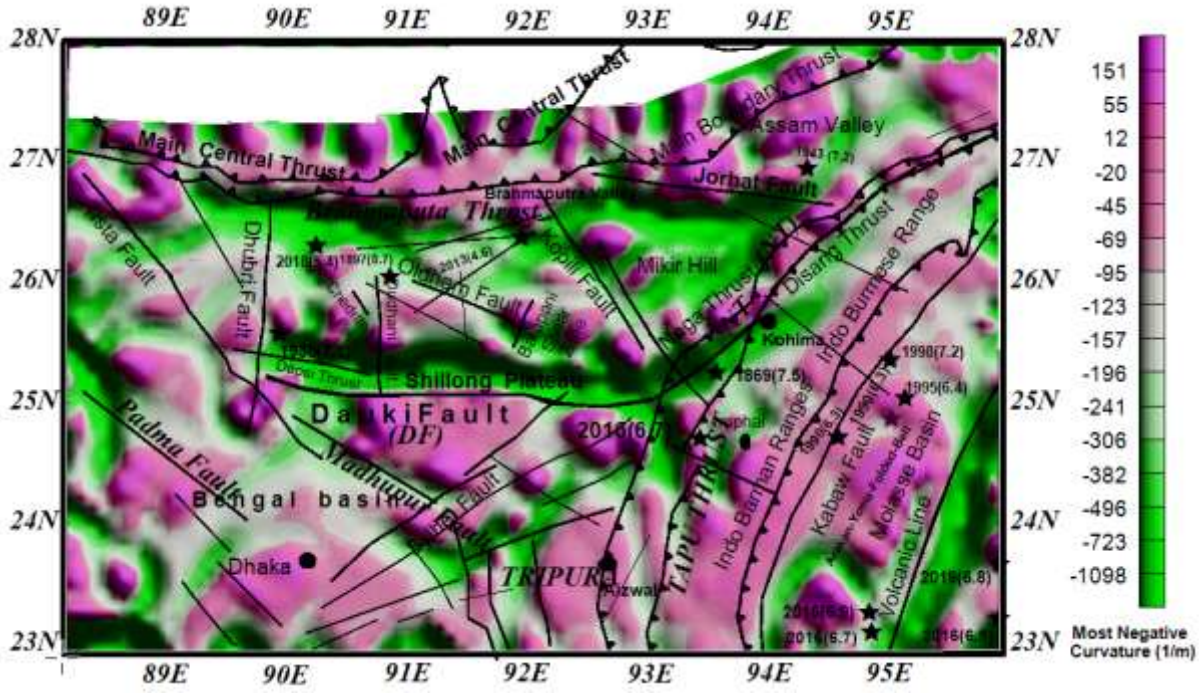


Fig. 15. Map shows the most negative curvature ( $K_{-}$ ) which indicates the greatest negative values (green colour) and also specifies the exteame synclinal and bowl features. Most negative curvature plot is superimposed on the tectonic map. Study suggests that the color contract patterns (green colour) are matching along with the thrust-fault locations.

The results are very encouraging and helps for direct delineation of thrust/ fault locations. In order to better correlationa and comparative analysis, all the results (most negative curvature, source edge locations abd Euler source depth locations are plotted as shown in **Figure 18**. Study suggests the most negative curvature (green color contrast patterns) are matching along with the thrust-fault locations/ lineaments derived by the past researchers (**Ghosh, 2019 and 2022).**

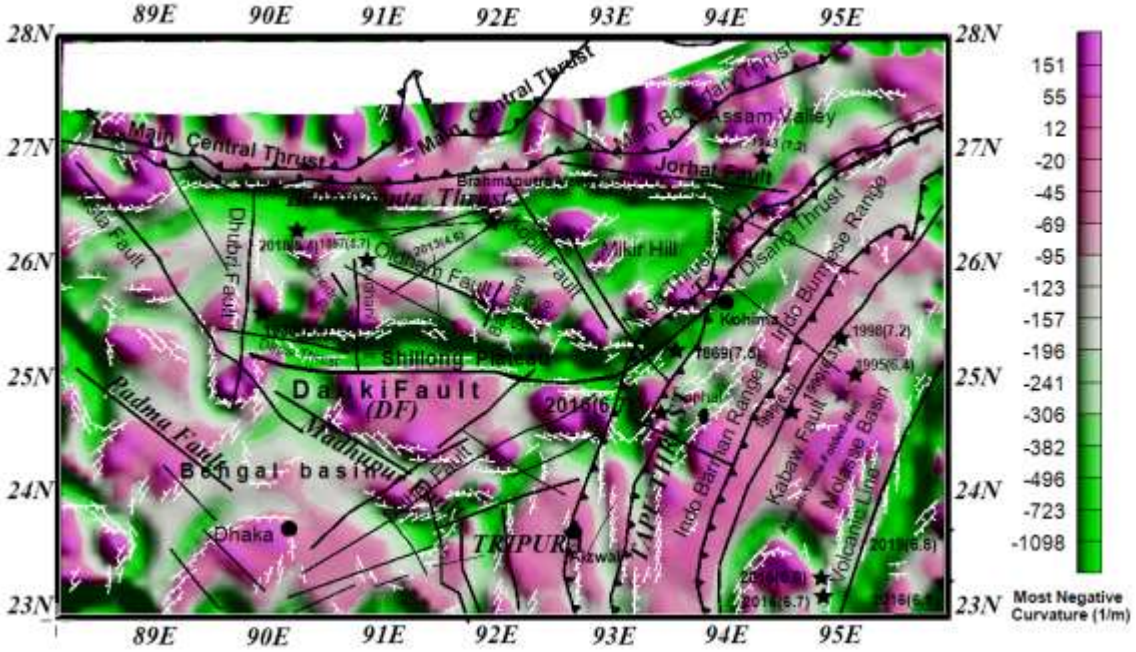


Fig. 16. Map shows the source edge locations (marked as white linnes) (**Ghosh, 2019**) superimposed on the most negative curvature plot (green colour contrast) are well correlating.

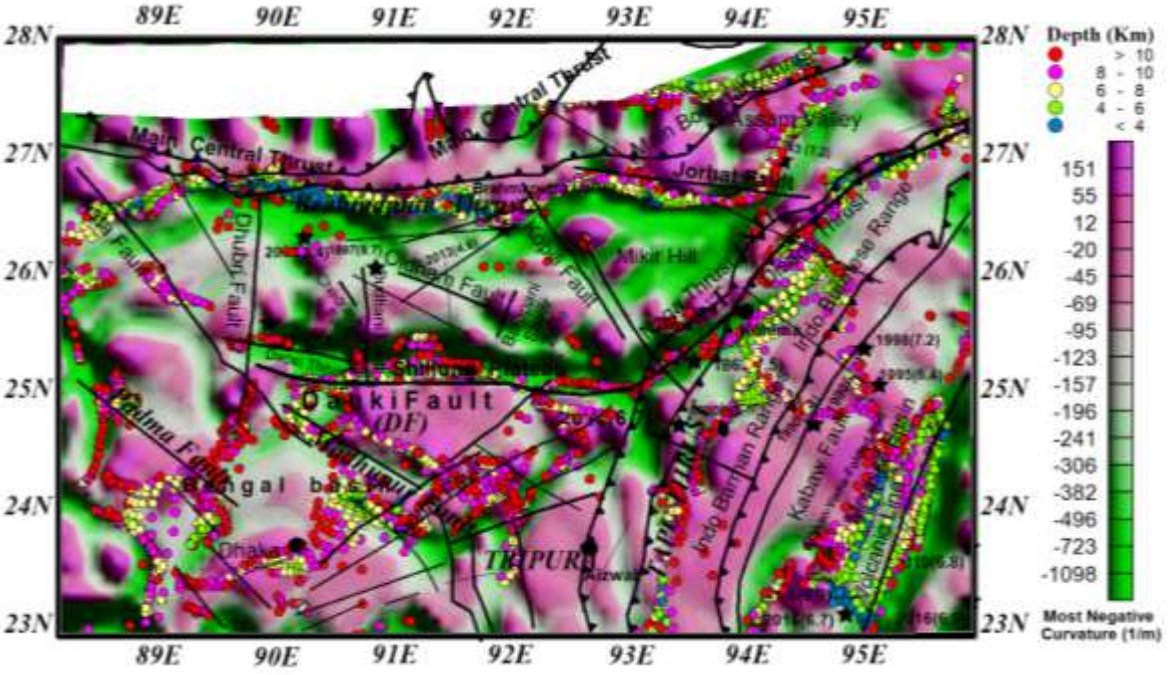


Fig. 17. Map shows the most negative curvature plot superimposed on the three-dimensional Euler source depth locations (marked with different colour circles) (**Ghosh, 2022)**.

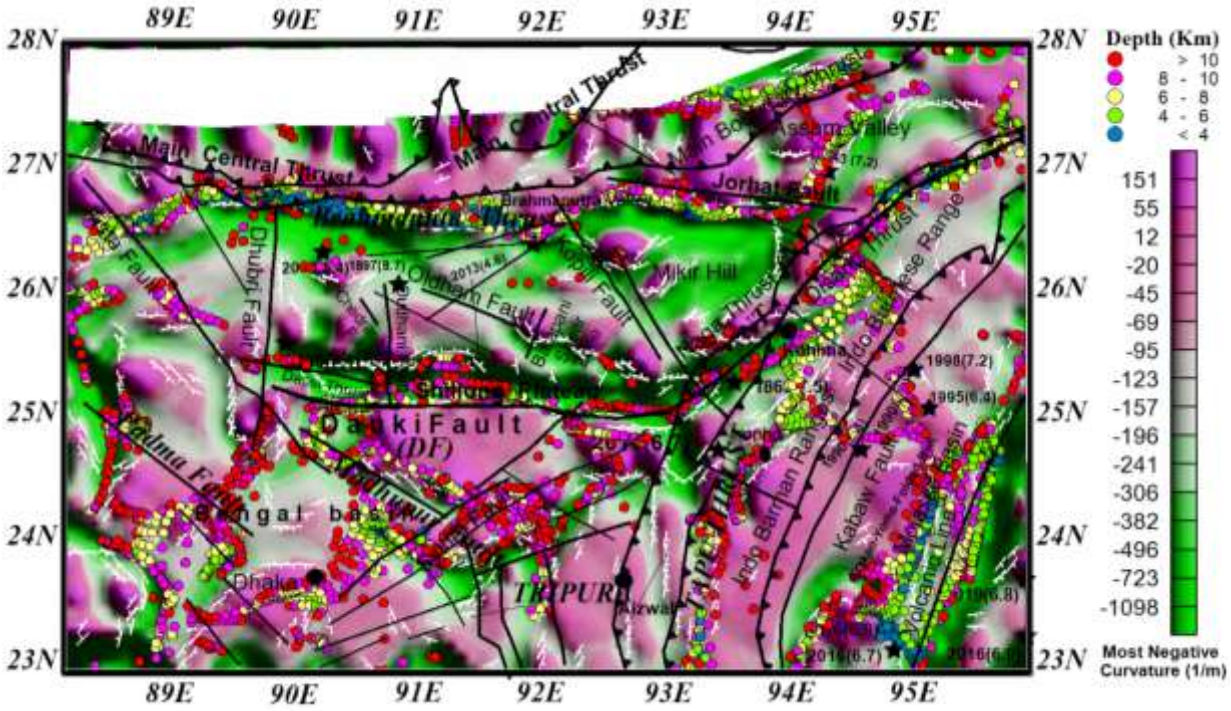


Fig. 18. Map shows the most negative curvature plot superimposed on the source edge locations **(Ghosh 2019)** and three-dimensional Euler source depth location **(Ghosh, 2022)**.

The results derived by the most positive curvature and the most negative curvature are well correlated with the past studies and proving a siginificant role for providing thrust-fault delineation.

## Summary and Conclusions

Most positive and most negative curvature interpretations have been carried out in one of the utmost seismically vigorous zones covering latitude 23°–28°N and longitude 88°–96°E in the north-eastern part of India. The area of study has very scanty and limited information of thrust-fault. In this study, most positive and most negative curvature attributes are interpreted for understanding sub-surface structural features and identify structural lineament/thrust-fault using ground gravity data and provided a integral view.

Curvature interpretation are correlated and compared with the past studied like three-dimensional Euler source depth locations (**Ghosh 2022**) and source edge locations **(Ghosh 2019**). The combined outcomes of the curvature interpretations providing a good result to delineate the thrust–fault locations.

The most positive curvature ( $K_+$ ) plot shows the greatest positive value and show anticlinal and domal features as marked with the purple color (**Fig. 11).** The above study suggests that the results derived by the three-dimensional Euler deconvolution by **Ghosh (2022**) and source edge pattern derived by **Ghosh (2019)** are well correlated and matching with results from the most positive curvature **(Fig. 14**). The results are very encouraging and helps for direct delineation of thrust/ fault locations. It is to be noted that there are some additional purple colour contrasts indicated in the most positive curvature plot might be probable additional lineament/thrust-fault locations. Similarly, most negative curvature ( $K_-$ ) (**Fig. 15**), designates the greatest negative values as marked with green colour contrast stipulates the extreme synclinal and the bowl shape feature. Both the plots (most negative and the most positive curvatures) highlighted the lineament/fault pattern in the geometric surface and well supported correlated with the previous work carried by **Ghosh (2022, 2019).** The colour contrast in the most positive curvature (purple colour) and most negative curvatures (green colour) plots are clearly indicating the delineation pattern. The study also suggests some additional colour contrast plot may provide supplementary new thrust-fault/ lineament and can be helpful for better and further geoscientific study. As gravity data has its own constraints, hence additional information and other geoscientist data can provide more precise information in the study area.

411 **Acknowledgement**

412

413 I thank to the various authors of the journals/text directly or indirectly for their ideas and
414 inspiration during the course of the work. I also thank the anonymous reviewers/editor
415 for their useful comment.

416

417 **Conflict of interest:** The corresponding author states that there is no conflict of interest.

418

419 **References**

420

421 Ambraseys N, Douglas J 2004 Magnitude calibration of north Indian N. earthquakes.
422 Geophys J Int 159:165–206

423 Awasthi N, Ray J, Singh, A K, Band ST, Rai V K 2014 Provenance of the late quaternary
424 sediments in the Andaman Sea: implications for monsoon variability and ocean
425 circulation. Geochem Geophys Geosyst 15:3890–3906.
426 https://doi.org/10.1002/2014G C005462

427 Bansal B K, Verma M 2013 Science and technology-based earthquake risk reduction
428 strategies: the Indian scenario. Acta Geophys 61(4):808–821.
429 https://doi.org/10.2478/s11600-013-0105-5

430 Bilham R, England P 2001 Plateau 'pop up' in the great, 1897, Assam earthquake.
431 Nature 410:806–809

432 Biswas S and Grasemann B 2005 Quantitative morphotectonics of the southern Shillong
433 Plateau (Bangladesh/ India); Austr. J. Earth Sci. 97 82–93.

Devi N R and Sarma K P 2010 Strain analysis and stratigraphic status of Nongkhya, Sumer and Mawmaram conglomerates of Shillong basin, Meghalaya, India. Jour. Earth System Sci., v.119, pp.161–174. https://www.ias.ac.in/article/fulltext/jess/119/02/0161-0174.

Evans P 1964 The Tectonic framework of Assam, J. Gel. Soc. India, 5, pp 80-96.

Fairhead J D, Salem A, Cascone L, Hammil M, Masterton S, Samson E 2011 New developments of the magnetic tilt-depth methodto improve structural mapping of sedimentary basins. Geophys Prospect 59:1072–1086. https://doi.org/10.1111/j.1365-2465-2478. 2011.01001.x

Fedi M 2007 DEXP: a fast method to determine the depth and the structural index of potential fields sources. Geophysics 72(1): I1–I11. https://doi.org/10.1190/1.2399452

FitzGerald D, Reid A B, McInerney P 2004 New discrimination techniques for Euler deconvolution. Comput. Geosci. 30(5):461–469. https://doi.org/10.1016/j.cageo.2004.03.006

Ghosh G K and Dasgupta R 2013 Edge detection and depth estimation using 3D Euler deconvolution, Tilt angle derivative and TDX derivative using magnetic data of thrust fold belt area of Mizoram, Society of Petroleum Geophysicists, 10th Biennial International Conference & Exposition,

Ghosh G K 2015 Interpretation of gravity anomaly and crustal thickness mapping of Narmada-Son lineament in central India, Journal of the Geological Society of India, Vol 86(3), pp:263-274.

456 Ghosh G K 2016a Magnetic Data Interpretation for the Source-Edge Locations in Parts
457 of the Tectonically Active Transition Zone of the Narmada-Son Lineament in
458 Central India. Pure Appl. Geophys. 173, 555–571 (2016).
459 https://doi.org/10.1007/s00024-015-1082-1

460 Ghosh G K 2016b Interpretation of Gravity Data using 3D Euler Deconvolution, Tilt
461 Angle, Horizontal Tilt Angle and Source Edge Approximation of the North-West
462 Himalaya, Acta Geophysica 64 (4), 1112-1138. https://doi.org/10.1515/acgeo-
463 2016-0042

464 Ghosh G K 2018 Automatic Delineation of Structural Boundaries using Curvature
465 Analysis of Bouguer Gravity Data in Parts of Northwest Himalaya, Journal of
466 Geological Society of India 91 (5), 589-595.

467 Ghosh G K 2019 Interpretation of gravity anomaly to delineate thrust faults locations at
468 the northeastern part of India and its adjacent areas using source edge detection
469 technique, tilt derivative and Cos(θ) analysis. Acta Geophys. 67, pp.1277–1295.
470 https://doi.org/10.1007/s11600-019-00345-8.

471 Ghosh G K 2020 Curvature interpretation of gravity data for delineating structural
472 features across the transition zone of Narmada–Son lineament in central India. J
473 Earth Syst Sci 129-142. https://doi.org/10.1007/s12040-020-01402-3

474 Ghosh G K 2022 Evidence of major subsurface structural features and source depth
475 locations using three-dimensional Euler deconvolution of ground gravity data at the
476 north-eastern part of India Journal Acta Geophysica, 1-9,
477 https://doi.org/10.1007/s11600-022-00829-0 (In press).

478 Ghosh G K, Basha S K, Salim Md and Kulshreshth V K 2010 Integrated interpretation
479 of seismic, gravity, magnetic and magneto-telluric data in geologically complex
480 thrust belt areas of Manabum, Arunachal Pradesh, J. Ind. Geophys. Union, Vol.14,
481 No.1, pp.1-14.

482 Ghosh G K, Dasgupta R, Reddy B J and Singh S N 2015 Gravity data interpretation
483 across the Brahmaputra Thrust and Dauki Fault in the north-eastern India, Journal
484 of Geophysics 36, 31-38.

485 Ghosh G K, Manda K L, Rao G V J 2017 Estimation of Geological Boundary and Source
486 Depth Locations Using Seismic, Gravity, Magnetic and Geochemical Data in
487 Assam-Arakan Basin in Mizoram State of N-E India, GEOHORIZONS July, pp:1-
488 6.

489 Ghosh G K, Mandal K L, Rao G V J, Basha SK 2017 Delineating Subsurface Structures
490 using Curvature Analysis of Gravity Data in parts of Thrust-fold Belt Area of Assam-
491 Arakan Basin in Mizoram State, North Eastern India Jour. of Geophysics 38 (2),
492 101-110

493 Ghosh G K, Singh C L 2011 Shallow Crustal Configuration of the Narmada–Son
494 Lineament Transition Zone Near the Sahdol–Katni Area of Central India Using
495 Simultaneous Gravity and Magnetic Observations. Pure Appl. Geophys. 168, 845–
496 860 https://doi.org/10.1007/s00024-010-0174-1

497 Harijan N, Sen AK, Sarkar S, Das JD, Kanungo DP 2003 Geomorphotectonics around
498 the Sung valley carbonatite complex, Shillong plateau, NE India: remote sensing
499 and GIS approach. J Geol Soc India 62(1):103–109

Hazarika D, Kundu A and Ghosh P 2022 Seismotectonic scenario of the indenting northeast corner of the Indian plate in the Tidding-Tuting Suture Zone of the Eastern Himalayan Syntaxis, Tectonophysics, Volume 824, Feb 2022, 229197, https://doi.org/10.1016/j.tecto.2021.229197.

Kayal J R 2001 Microearthquake activity in some parts of the Himalaya and the tectonic model. Tectonophysics 33

Kayal J. R, Arefiev S S, Barua S, Hazarika D, Gogoi N, Kumar A, Chowdhury S N, and Kalita S 2006 Shillong Plateau Earthquakes in Northeast India Region: Complex Tectonic Model, Current Science, 91, no.1, 109-114. http://www.jstor.org/stable/24094186.

Khan P K, Chakraborty P P 2007 The seismic b-value and its correlation with Bouguer gravity anomaly over the Shillong Plateau area: Tectonic implications, Journal of Asian Earth Sciences,Volume 29, Issue 1, 136-147, https://doi.org/10.1016/j.jseaes.2006.02.007

Klingele E E, Marson I, Kahle HG 1991 Automatic interpretation of gravity gradiometric data in two dimensions: vertical gradient. Geophys Prospect 39:407–434. https://doi.org/10.1111/j.1365-2478. 1991.tb00319.x

Lee M D Morris B Leblanc G and Harris 2012 Curvature analysis for geological mapping and mineral resource assessment: 82nd Annual International Meeting; SEG, Expanded Abstracts. doi: 10.1190/segam2012-1358.1.

Li Xiong 2015 Curvature of a geometric surface and curvature of gravity and magnetic anomalies; Geophysics 80 G15–G26. doi:10.1190/geo2014-0108.1.

522 Marson I, Klingele EE 1993 Advantages of using the vertical gradient of gravity for 3-D
523 interpretation. Geophysics 58(11):1588–1595. https://doi.org/10.1190/1.1443374

524 Mclay K R, Bonora M 2001 Analog models of restraining stopovers in strike–slip fault
525 systems. Am Assoc Pet Geol Bull 85:233–260

526 Mikhailov V, Galdeano M, Gvishiani A, Agayan S, Bogoutdinov S, Graeva E, Sailhac P
527 2003 Application of artifcial intelligence for Euler solutions clustering. Geophysics
528 68(1):168–180. https:// doi.org/10.1190/1.1543204

529 Mishra, M. and Sen Shinjana 2010 Geochemistry and origin of Proterozoic Porcellanitic
530 Shales from Chopan, Vindhyan Basin, India, Indian Journal of Geology, 80, Nos.
531 1-4, 157-171.

532 Mitra S K 1998 Structure, sulphide mineralization and age of the Shillong group of rocks,
533 Meghalaya. In: M.S. Krishnan Commemorative National Seminar. 1 and 2 Nov.,
534 Kolkata, pp.118–119.

535 Nandy R and Dasgupta S 1991 Seismotectonic domains of northeastern India and
536 adjacent areas, Physics and Chemistry of the Earth, Volume 18, Part 1,371-
537 384,https://doi.org/10.1016/0079-1946(91)90010-D.

538 Oldham R D 1899 Report of the great earthquake of 12th June. Mem Geol Surv India
539 46:257–276

540 Peet F G and Sahota T S 1985 Surface curvature as a measure of image texture; IEEE
541 Transactions on Pattern Analysis and Machine Intelligence PAM1; 7(6) 734-738.

542 Rajendran C P, Rajendran K, Duarah B P, Baruah S and Earnest A 2004 Interpreting
543 the style of faulting and paleoseismicity associated with the 1897 Shillong,
544 northeast India, earthquake: Implications for regional tectonism, Tectonics, 23,
545 TC4009, doi:10.1029/2003TC001605.

546 Rajesekhar R P, Mishra D C 2008 Crustal structure of Bengal Basin and Shillong
547 Plateau: extension of Eastern Ghat and Satpura Mobile Belts to Himalayan fronts
548 and seismotectonics. Gondwana Res. https://doi.org/10.1016/j.gr.2007.10.009

549 Rao N P, Kumar P, Tsukuda T, Ramesh DS 2006 The devastating Muzafarbad
550 earthquake of 8 October 2005: new insights into Himalayan seismicity and
551 tectonics. Gondwana Res 9:365–378

552 Ravi Kumar Ch, Selin Raj A, Pathak B, Saumen Maiti, Naganjaneyulu K. 2020 High
553 density crustal intrusive bodies beneath Shillong plateau and Indo Burmese Range
554 of northeast India revealed by gravity modeling and earthquake data, Physics of
555 the Earth and Planetary Interiors, 307, 106555,
556 https://doi.org/10.1016/j.pepi.2020.106555

557 Reid A B, Fitzgerald D, and Mcinerny P 2003 Euler deconvolution of gravity data: 73rd
558 488 Annual International Meeting; SEG, Expanded Abstracts, pp 580–583

559 Reid AB, Ebbing JO, Susan SJ 2014 Avoidable Euler errors—the use and abuse of
560 Euler deconvolution applied to potential fields. Geophys Prospect 62(5):1162–
561 1168. https://doi.org/10.1111/1365-2478.12119

562 Roberts A 2001 Curvature attributes and their applications to 3D interpreted horizons;
563 First Break 19 85–100. doi: 10.1046/j.02635046.2001.00142.x.

564 Robinson R A J, Brezina C A, Parrish R R, Horstwood MSA, Oo NW, Bird MI, Thein M,
565 Walters A.S. G, Oliver J.H, Zaw, K., 2014 Large rivers and orogens: the evolution
566 of the Yarlung TsangpoIrrawaddy system and the eastern Himalayan syntaxis.
567 Gondwana Res 26:112–121. https://doi.org/10.1016/j.gr.2013.07.002.

568 Roy L, 2008 Constrained Inversion of Gravity Data Over Shillong Plateau, 7th
569 International conference and exhibition on petroleum Geophysics, Soc. Pet.
570 Geophysicist, Paper no 141, 1-5.

571 Saibi H, Nishijima J, Ehara S, Essam A 2006 Integrated gradient interpretation
572 techniques for 2D and 3D gravity data interpretation. Earth Planet Sp 58:815–821.
573 https://doi.org/10.1186/BF033 51986

574 Salem A, Williams S, Fairhead J D, Ravat D, Smith R 2007 Tiltdepth method; A simple
575 depth estimation method using frst-order magnetic derivatives. SEG the Leading
576 Edge 26/12:1502–1505

577 Schellart W P, Nieuwland D A 2003 3D evolution of a pop-up structure above a double
578 basement strike–slip fault: some insights from analogue modelling. In: Nieuwland
579 DA (ed) New insights into structural interpretation and modelling. Geological
580 Society Special Publications, London, pp 169–179. https://doi.org/10.1144/
581 GSL.SP.2003.212.01.11

582 Seno T, Rehman H U 2011 When and why the continental crust is subducted: examples
583 of Hindu Kush and Burma. Gondwana Res 19:327–333

584 Shukla N, Hazarika D, Kundu A, Mukhopadhyay S 2022 Spatial variations of crustal
585 thickness and Poisson's ratio in the northeastern region of India based on receiver

function analysis, Geological Journal, First published: 10 May 2022, https://doi.org/10.1002/gj.4469

Silva JBC, Barbosa VCF 2003 3D Euler deconvolution: theoretical basis for automatically selecting good solutions. Geophysics 68(6):1962–1968. https://doi.org/10.1190/1.1635050

Slotnick M M 1932 Curvature of equipotential surfaces; AAPG Bulletin 16 1250–1259.

Thomas G B 1972 Calculus and analytic geometry, 4th ed.: Addison- Wesley Co.

Thurston J B and Smith R S 1997 Automatic conversion of magnetic data to dep, dip and susceptibility contrast using the SPI™ method; Geophysics 62 807–813.

Verma R K, Mukhopadhay M 1977 An analysis of the gravity field in north-eastern India. Tectonophysics 42:283–317

Wang W, Pan Y, Qiu Z 2009 A new edge recognition technology based on the normalized vertical derivative of the total horizontal derivative for potential feld data. Appl Geophys 6(3):226–233. https://doi.org/10.1007/s11770-009-0026-x

Wijns C, Perez C, Kowalczyk P 2005 Theta Map: edge detection in magnetic data. Geophysics 70: L39–L43. https://doi.org/10. 1190/1.2194525

Yadav R B S, Bormann P, Rastogi, B K, Das M C and Chopra S 2009 A homogeneous and complete earthquake catalog for northeast India and the adjoining region, Seism. Res. Lett. 80(4), 609–627

Yaghoobian A, Boustead GA, Dobush T M 1992 Object delineation using Euler's homogeneity equation: location and depth determination of buried ferro-metallic

607 bodies. In: Proc. Symp. on Application of Geophysics to Engineering and
608 Environmental Problems 1993, San, USA, pp 613–632 Diego. https://doi.org/10.
609 4133/1.2922042

610 Young M 1978 Statistical characterisation of attribute matrices by computer. The fifth
611 progress report on Contract DA-ERO-591-73-G0040. U.S. Army European
612 Research Office, London. Report 5, 1-16.

613
614 **Views expressed in this paper are that of authors only, and may not necessarily be
615 of OIL.